Control Proxy Functions for Sequential Design and Control Optimization

Diane L. Peters[1]
e-mail: dlpeters@umich.edu

P. Y. Papalambros
e-mail: pyp@umich.edu

A. G. Ulsoy
e-mail: ulsoy@umich.edu

University of Michigan,
2250 G. G. Brown Building,
2350 Hayward Street,
Ann Arbor, MI 48109

Optimal system design of "smart" products requires optimization of both the artifact and its controller. When the artifact and the controller designs are independent, the system solution is straightforward through sequential optimization. When the designs are coupled, combined simultaneous optimization can produce system-optimal results, but presents significant computational and organizational complexity. This paper presents a method that produces results comparable with those found with a simultaneous solution strategy, but with the simplicity of the sequential strategy. The artifact objective function is augmented by a control proxy function (CPF), representing the artifact's ease of control. The key to successful use of this method is the selection of an appropriate CPF. Four theorems that govern the choice and evaluation of a CPF are given. Each theorem is illustrated using a simple mathematical example. Specific CPFs are then presented for particular problem formulations, and the method is applied to the optimal design and control of a micro-electrical mechanical system actuator. [DOI: 10.1115/1.4004792]

Keywords: co-design, optimization, coupling, control

1 Introduction

Optimal design of "smart" products and systems requires optimization of both the physical system or artifact, and its controller. This codesign problem can present challenges when the design of artifact and controller is dependent on each other. In general, the artifact objective function, f_a, and inequality and equality constraints, $\boldsymbol{g}_a$ and $\boldsymbol{h}_a$, may all be functions of both artifact and control variables, $\boldsymbol{d}_a$ and $\boldsymbol{d}_c$, respectively. Likewise, the control objective function, f_c, and inequality and equality constraints, $\boldsymbol{g}_c$ and $\boldsymbol{h}_c$, may all be functions of both $\boldsymbol{d}_a$ and $\boldsymbol{d}_c$; i.e., $f_a = f_a(\boldsymbol{d}_a, \boldsymbol{d}_c)$, $\boldsymbol{g}_a = \boldsymbol{g}_a(\boldsymbol{d}_a, \boldsymbol{d}_c)$, $\boldsymbol{h}_a = \boldsymbol{h}_a(\boldsymbol{d}_a, \boldsymbol{d}_c)$, $f_c = f_c(\boldsymbol{d}_a, \boldsymbol{d}_c)$, $\boldsymbol{g}_c = \boldsymbol{g}_c(\boldsymbol{d}_a, \boldsymbol{d}_c)$, and $\boldsymbol{h}_c = \boldsymbol{h}_c(\boldsymbol{d}_a, \boldsymbol{d}_c)$. When this interdependence exists, the solution of the bi-objective optimization problem given by Eqs.(1)–(5) is a Pareto set, with the various Pareto points found by varying the weights w_a and w_c, where $w_a, w_c > 0$, and the problem is said to be coupled.

$$\min_{\boldsymbol{d}_a, \boldsymbol{d}_c} w_a f_a + w_c f_c \tag{1}$$

$$\text{subject to } \boldsymbol{g}_a \leq \boldsymbol{0} \tag{2}$$

$$\boldsymbol{h}_a = \boldsymbol{0} \tag{3}$$

$$\boldsymbol{g}_c \leq \boldsymbol{0} \tag{4}$$

$$\boldsymbol{h}_c = \boldsymbol{0} \tag{5}$$

Many such coupled systems have been reported in the literature. These include structural systems with active control (e.g., Refs. [1–3]), micro-electrical mechanical systems (MEMS, e.g., Refs. [4, 5]), and robotics and mechatronics (e.g., Refs. [6–8]). The experimental and analytical studies have shown that coupling must be considered and addressed and that doing so can present significant challenges (e.g., Refs. [9–12]).

When all of the objective and constraint functions depend on both $\boldsymbol{d}_a$ and $\boldsymbol{d}_c$, coupling is described as bi-directional. However, there are many engineering problems in which the artifact objective and constraints are not functions of $\boldsymbol{d}_c$, i.e., $f_a = f_a(\boldsymbol{d}_a)$, $\boldsymbol{g}_a = \boldsymbol{g}_a(\boldsymbol{d}_a)$, and $\boldsymbol{h}_a = \boldsymbol{h}_a(\boldsymbol{d}_a)$. Such problems include many structures subject to active control (e.g., Ref. [13]); other such systems exists, including an elevator with gain-scheduled control [14]. Coupling in these problems is described as unidirectional. In the present work, only unidirectional coupling is considered.

A variety of measures have been proposed to quantify the strength of coupling [1,15–17]. These measures have been shown to be related, though most are not commensurate with one another [18,19]. In problems with unidirectional coupling, a useful measure is the coupling vector, $\boldsymbol{\Gamma}_v$, which will be used in this work, and is defined as Refs. [16, 20, 21]:

$$\Gamma_v = \frac{w_c}{w_a}\left(\frac{\partial f_c}{\partial \boldsymbol{d}_a} + \frac{\partial f_c}{\partial \boldsymbol{d}_c}\frac{\partial \boldsymbol{d}_c}{\partial \boldsymbol{d}_a}\right) \tag{6}$$

This vector is valid only at an optimal solution; however, if a point is not known to be an optimal solution, an estimate can be computed. The equation for the estimated coupling vector, denoted as $\widehat{\Gamma}_v$, is identical to Eq. (6), but does not require the solution of Eqs. (1)–(5). Of course, if the point does happen to be on the Pareto frontier, then $\widehat{\Gamma}_v = \Gamma_v$.

It has been shown that simple sequential optimization, in which the artifact is first optimized and then the optimal control is found for that artifact, does not necessarily find system-optimal solutions [21,22]. Combined optimization methods such as a simultaneous strategy, in which both the artifact and the control are optimized together, will produce system-optimal solutions [21,22]. These methods require combining expertise from more than one discipline to formulate and solve the full optimization problem. This presents organizational challenges, since such expertise is typically found in different individuals or different groups within an organization. Furthermore, specialized techniques developed for optimal control can no longer be used when the problem is not formulated as a purely optimal control one. The combined solution presents also a computational challenge.

In this paper, the new concept of a control proxy function (CPF) is introduced. A combined problem including the CPF and the artifact objective function is formulated, followed by the optimization of the control problem. This allows an effective sequential solution strategy to be implemented for the combined problem. The CPF concept is introduced in Sec. 2. In Sec. 3, four theorems are presented governing the choice and the evaluation of appropriate CPFs, and simple mathematical examples are used to

[1]Corresponding author.

Contributed by the Design Automation Committee of ASME for publication in the JOURNAL OF MECHANICAL DESIGN. Manuscript received May 25, 2010; final manuscript received June 17, 2011; published online September 15, 2011. Assoc. Editor: Timothy W. Simpson.

demonstrate the concepts. In Sec. 4, the use of a CPF is shown to provide optimal or near-optimal solutions to the codesign problem without the disadvantages seen in the combined optimization techniques. A set of CPFs are derived for the specific problem formulations. In Sec. 5, the method is demonstrated on a MEMS actuator, and Sec. 6 presents concluding remarks.

2 Control Proxy Function Problem Formulation

In order to preserve the functional decomposition of the codesign problem while realizing optimal or near-optimal solutions, a modified sequential optimization strategy is proposed. In this strategy, the original artifact objective function, f_a, is augmented with a CPF, representing the system's ease of control. The CPF, denoted as χ, is a function of only the artifact design variables $\boldsymbol{d}_a$; it is independent of the control design variables $\boldsymbol{d}_c$ and of the control architecture itself. The bi-objective artifact design problem with the two functions $f_a(\boldsymbol{d}_a)$ and $\chi(\boldsymbol{d}_a)$ may be solved in a variety of ways, as discussed in the multi-objective optimization literature (e.g., Refs. [23–26]). In this paper, a simple weighted linear combination will be used to demonstrate the proposed method. The optimization problem is then formulated as follows, see Fig. 1:

$$\min_{\boldsymbol{d}_a} w_1 f_a(\boldsymbol{d}_a) + w_2 \chi(\boldsymbol{d}_a) \tag{7}$$

$$\text{subject to } \boldsymbol{g}_a(\boldsymbol{d}_a) \le \boldsymbol{0} \tag{8}$$

$$\boldsymbol{h}_a(\boldsymbol{d}_a) = \boldsymbol{0} \tag{9}$$

where the positive weights w_1 and w_2 represent the relative importance of the artifact objective and the CPF. This is followed by the control design problem:

$$\min_{\boldsymbol{d}_c} f_c(\boldsymbol{d}_a^*, \boldsymbol{d}_c) \tag{10}$$

$$\text{subject to } \boldsymbol{g}_c(\boldsymbol{d}_a^*, \boldsymbol{d}_c) \le \boldsymbol{0} \tag{11}$$

$$\boldsymbol{h}_c(\boldsymbol{d}_a^*, \boldsymbol{d}_c) = \boldsymbol{0} \tag{12}$$

where $\boldsymbol{d}_a^* = \text{argmin}(w_1 f_a(\boldsymbol{d}_a) + w_2 \chi(\boldsymbol{d}_a))$ subject to $\boldsymbol{g}_a(\boldsymbol{d}_a) \le \boldsymbol{0}$, $\boldsymbol{h}_a(\boldsymbol{d}_a) = \boldsymbol{0}$ is the solution to Eqs. (7)–(9).

The success of the method, in terms of reproducing the results of the simultaneous formulation of Eqs. (1)–(5), depends on the selection of an appropriate CPF. A well-chosen CPF, which effectively captures the fundamental physical limitations that determine the attainable control performance of the system, will result in solutions close to the Pareto-optimal points found by a simultaneous formulation; a poorly chosen CPF will yield solutions far from system optimality. The question then arises of how one should choose an appropriate CPF, and how one may evaluate a proposed CPF to determine whether it results in optimal or near-optimal solutions. Of course, the closeness of the CPF solution should be determined without solving the simultaneous formulation in Eqs. (1)–(5) for Pareto optimal points, since the motivation for the CPF formulation is to eliminate the need to solve the simultaneous problem.

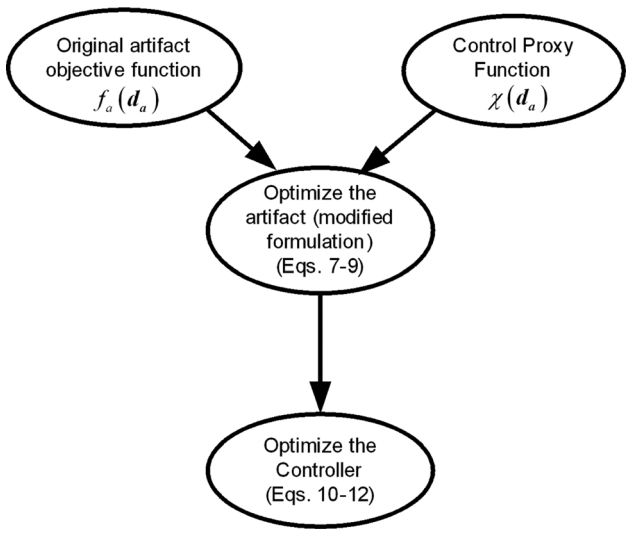

Fig. 1 Control proxy function problem formulation

3 Characteristics of Effective Control Proxy Functions

Four theorems are presented that govern the characteristics of an appropriate CPF. First, a "perfect" CPF is defined, and a condition which ensures that a CPF is perfect is given as Theorem 1. Next, for a CPF that is not perfect, a measure of its "closeness" to the Pareto frontier is defined and characterized in Theorem 2. Finally, Theorems 3 and 4 relate an effective CPF to the mathematical form of the control objective function, f_c. For Theorems 2 through 4, it is assumed that all functions are locally convex.

3.1 Characterization of a Perfect CPF. A CPF is described as perfect if every solution of the CPF problem is also a solution to the simultaneous problem given in Eqs. (1)–(5), i.e., every CPF point will coincide with the Pareto frontier. Such points satisfy the condition given in Theorem 1.

Theorem 1. *If $\Gamma_v \parallel \nabla\chi$ for all solutions to the CPF problem given in Eqs. (7)–(9), then all solutions to the CPF problem will also be solutions to the simultaneous problem given in Eq. (1)–(5).*

Proof. For the simultaneous problem stated in Eqs. (1)–(5), the Karush-Kuhn-Tucker (KKT) conditions [27] can be stated as

$$\begin{bmatrix} \dfrac{\partial f_a}{\partial \boldsymbol{d}_a} + \dfrac{w_c}{w_a}\left(\dfrac{\partial f_c}{\partial \boldsymbol{d}_a} + \dfrac{\partial f_c}{\partial \boldsymbol{d}_c}\dfrac{\partial \boldsymbol{d}_c}{\partial \boldsymbol{d}_a}\right) \\ \dfrac{w_c}{w_a}\dfrac{\partial f_c}{\partial \boldsymbol{d}_c} \end{bmatrix} + \boldsymbol{\lambda}^T \begin{bmatrix} \dfrac{\partial \boldsymbol{h}_a}{\partial \boldsymbol{d}_a} \\ \dfrac{\partial \boldsymbol{h}_c}{\partial \boldsymbol{d}_c} \end{bmatrix} + \boldsymbol{\mu}^T \begin{bmatrix} \dfrac{\partial \boldsymbol{g}_a}{\partial \boldsymbol{d}_a} \\ \dfrac{\partial \boldsymbol{g}_c}{\partial \boldsymbol{d}_c} \end{bmatrix} = \boldsymbol{0} \tag{13}$$

$$\boldsymbol{\mu}^T \begin{bmatrix} \boldsymbol{g}_a \\ \boldsymbol{g}_c \end{bmatrix} = \boldsymbol{0}, \quad \boldsymbol{\lambda} \ne \boldsymbol{0}, \quad \boldsymbol{\mu} \ge \boldsymbol{0} \tag{14}$$

and, for the CPF problem stated in Eqs. (7)–(12), the KKT conditions are

$$\begin{bmatrix} \dfrac{\partial f_a}{\partial \boldsymbol{d}_a} + \dfrac{w_2}{w_1}\dfrac{\partial \chi}{\partial \boldsymbol{d}_a} \\ \dfrac{w_2}{w_1}\dfrac{\partial f_c}{\partial \boldsymbol{d}_c} \end{bmatrix} + \boldsymbol{\lambda}^T \begin{bmatrix} \dfrac{\partial \boldsymbol{h}_a}{\partial \boldsymbol{d}_a} \\ \dfrac{\partial \boldsymbol{h}_c}{\partial \boldsymbol{d}_c} \end{bmatrix} + \boldsymbol{\mu}^T \begin{bmatrix} \dfrac{\partial \boldsymbol{g}_a}{\partial \boldsymbol{d}_a} \\ \dfrac{\partial \boldsymbol{g}_c}{\partial \boldsymbol{d}_c} \end{bmatrix} = \boldsymbol{0} \tag{15}$$

$$\boldsymbol{\mu}^T \begin{bmatrix} \boldsymbol{g}_a \\ \boldsymbol{g}_c \end{bmatrix} = \boldsymbol{0}, \quad \boldsymbol{\lambda} \ne \boldsymbol{0}, \quad \boldsymbol{\mu} \ge \boldsymbol{0} \tag{16}$$

Assume that, for every set of weights w_a and $\boldsymbol{W}_c$, there exists some set of weights w_1 and w_2 such that the two formulations will have identical solutions. Then it can be shown that

$$\frac{\partial f_a}{\partial \boldsymbol{d}_a} + \Gamma_v = \frac{\partial f_a}{\partial \boldsymbol{d}_a} + \frac{w_2}{w_1}\frac{\partial \chi}{\partial \boldsymbol{d}_a} \tag{17}$$

and, consequently, that

$$\Gamma_v = \frac{w_2}{w_1}\nabla\chi \tag{18}$$

Such a set of weights will exist and the modified sequential problem will produce the Pareto-optimal solutions when the gradient

of the CPF, $\nabla\chi$, is parallel to the coupling vector $\boldsymbol{\Gamma}_v$. Thus, the theorem is proven. □

Example. To illustrate the relationship between $\boldsymbol{\Gamma}_v$ and $\nabla\chi$, consider the following coupled optimization problem:

$$\min \quad w_a f_a(\boldsymbol{d}_a) + w_c f_c(\boldsymbol{d}_a, \boldsymbol{d}_c) \tag{19}$$

$$\text{subject to } g_a(\boldsymbol{d}_a) = 4d_{a_1}^2 + d_{a_2}^2 - 900 \le 0 \tag{20}$$

where

$$f_a = 0.5d_{a_1}^2 + d_{a_2}^2 - d_{a_1}d_{a_2} - 7d_{a_1} - 7d_{a_2} \tag{21}$$

$$f_c = (d_{a_1} - d_{a_2})^2 + \frac{1}{9}(d_{a_1} + d_{a_2} + \boldsymbol{d}_c - 10)^2 + (\boldsymbol{d}_c - 5)^2 \tag{22}$$

The CPF

$$\chi(\boldsymbol{d}_a) = 11d_{a_1}^2 + 11d_{a_2}^2 - 18d_{a_1}d_{a_2} - 10d_{a_1} - 10d_{a_2} + 25 \tag{23}$$

is chosen, and the system is optimized both sequentially and simultaneously.

The coupling vector $\boldsymbol{\Gamma}_v$ is given by the relation

$$\Gamma_v = \frac{2w_c}{9w_a}\begin{bmatrix} 10d_{a_1}^* - 8d_{a_2}^* + d_c^* - 10 \\ -8d_{a_1}^* + 10d_{a_2}^* + d_c^* - 10 \end{bmatrix}^T \tag{24}$$

where $d_{a_1}^*$, $d_{a_2}^*$, and d_c^* are values of these variables evaluated at an optimal solution. The CPF has the gradient

$$\nabla\chi = \begin{bmatrix} 22d_{a_1} - 18d_{a_2} - 10 \\ -18d_{a_1} + 22d_{a_2} - 10 \end{bmatrix}^T \tag{25}$$

Since there are no controller constraints $\boldsymbol{g}_c(\boldsymbol{d}_a, \boldsymbol{d}_c)$ or $\boldsymbol{h}_c(\boldsymbol{d}_a, \boldsymbol{d}_c)$, $\partial f_c/\partial \boldsymbol{d}_c = 0$ at an optimal solution, and therefore

$$d_c^* = 5.5 - 0.1d_{a_1}^* - 0.1d_{a_2}^* \tag{26}$$

Substituting into Eq. (24)

$$\Gamma_v = \frac{2w_c}{w_a}\begin{bmatrix} 1.1d_{a_1}^* - 0.9d_{a_2}^* - 0.5 \\ -0.9d_{a_1}^* + 1.1d_{a_2}^* - 0.5 \end{bmatrix}^T \tag{27}$$

Comparing Eqs. (25) and (27) at an optimal solution to the simultaneous problem, it can be seen that $\Gamma_v = 10\frac{w_c}{w_a}\nabla\chi$; therefore, the use of this CPF will duplicate the Pareto frontier.

3.2 Quantification of the "Closeness" of a CPF Point to the Pareto Frontier. As stated above, a perfect CPF is characterized by $\nabla\chi \parallel \Gamma_v$, i.e., when the angle ξ between the vectors $\nabla\chi$ and $\boldsymbol{\Gamma}_v$ is zero. This suggests that the angle ξ may serve as a means of evaluating the fidelity of a given CPF in modeling the behavior of f_c. The theorem specifies that no artifact constraints are active. However, since constraints reduce the degrees of freedom of a system, it is conjectured that if the problem is convex and the point in question is near the Pareto frontier, the angle ξ will represent an upper bound on the "distance" between a CPF point and the Pareto frontier when constraints are active.

Theorem 2. *If a codesign problem, as given in Eqs. (1)–(5), is convex and no artifact constraints $\boldsymbol{g}_a(\boldsymbol{d}_a)$, $\boldsymbol{h}_a(\boldsymbol{d}_a)$ are active, then the angle ξ between $\nabla\chi$ and the estimated coupling vector $\hat{\Gamma}_v$ at a CPF point will be monotonically related to ϵ, the distance between that CPF point and the nearest Pareto optimal point, measured in the $\boldsymbol{d}_a$-space.*

Proof. The distance from optimality has been defined in several ways [28]; here, it is defined as the distance between a given point, $\boldsymbol{d}_a$, and the nearest Pareto-optimal point, $\boldsymbol{d}_a^*$, in the $\boldsymbol{d}_a$-space

$$\varepsilon = \left\|\boldsymbol{d}_a - \boldsymbol{d}_a^*\right\|_2 \tag{28}$$

where $\boldsymbol{d}_a$ is the vector of design variables and $\boldsymbol{d}_a^*$ denotes the vector of design variables at an optimal solution to the codesign problem.

Since it has been specified that coupling is unidirectional, it is possible to express the optimal control design variables $\boldsymbol{d}_c$ as a function of the artifact design variables as follows:

$$d_c^* = \boldsymbol{d}_c(\boldsymbol{d}_a^*) \tag{29}$$

which allows the control objective f_c to be transformed into a function of only $\boldsymbol{d}_a$. This shall be used later in the proof in order to find gradients of f_c in the $\boldsymbol{d}_a$-space. It is possible to incorporate any active controller constraints $\boldsymbol{g}_c(\boldsymbol{d}_a, \boldsymbol{d}_c)$, $\boldsymbol{h}_c(\boldsymbol{d}_a, \boldsymbol{d}_c)$ into Eq. (29).

This codesign problem is also formulated as the CPF problem

$$\min_{\boldsymbol{d}_a} w_1 f_a(\boldsymbol{d}_a) + w_2\chi(\boldsymbol{d}_a) \tag{30}$$

followed by

$$\min_{\boldsymbol{d}_c} \quad f_c(\boldsymbol{d}_c) \tag{31}$$

$$\text{subject to} \quad \boldsymbol{g}_c(\boldsymbol{d}_c) \le \boldsymbol{0} \tag{32}$$

$$\boldsymbol{h}_c(\boldsymbol{d}_c) = \boldsymbol{0} \tag{33}$$

The functions $\chi(\boldsymbol{d}_a)$, $f_a(\boldsymbol{d}_a)$ and the reduced-space function $f_c(\boldsymbol{d}_a)$ are all assumed to be convex functions. Consider a point A which solves the CPF problem. At this point, with $\boldsymbol{d}_a = \boldsymbol{d}_a^A$

$$w_1\nabla f_a^A = -w_2\nabla\chi^A \tag{34}$$

The point B is chosen such that it is the nearest Pareto-optimal solution to point A. Its location in the artifact design variable space, therefore, satisfies the relation $\boldsymbol{d}_a^A = \boldsymbol{d}_a^B + \varepsilon\boldsymbol{v}$, where $\boldsymbol{v}$ is a unit vector normal to ∇f_a^B and ε is the distance between A and B, as shown in Fig. 2.

Using a Taylor series expansion of about B, the artifact and the controller objective functions at A can be expressed as

$$f_a^A = f_a^B + \nabla f_a^B\varepsilon\boldsymbol{v} + \frac{1}{2}\varepsilon^2\boldsymbol{v}^T\nabla^2 f_a^B\boldsymbol{v} + \text{higher order terms} \tag{35}$$

$$f_c^A = f_c^B + \nabla f_c^B\varepsilon\boldsymbol{v} + \frac{1}{2}\varepsilon^2\boldsymbol{v}^T\nabla^2 f_c^B\boldsymbol{v} + \text{higher order terms} \tag{36}$$

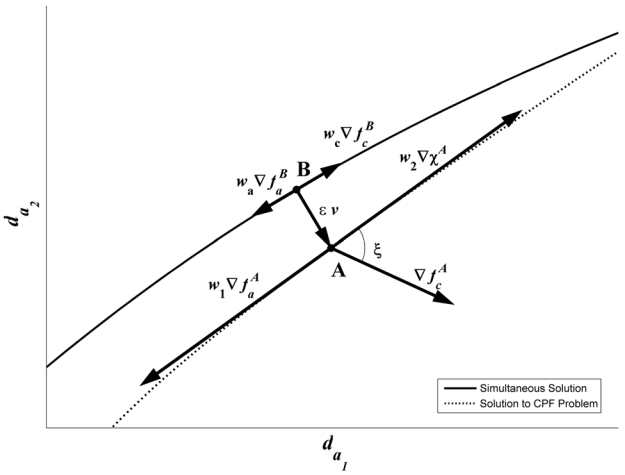

Fig. 2 Gradients at Points A and B

and, therefore, neglecting higher-order terms, the gradients of f_a and f_c at A can be expressed in terms of the gradients at B as

$$\nabla f_a^A = \nabla f_a^B + \varepsilon \boldsymbol{v}^T \nabla^2 f_a^B \tag{37}$$

$$\nabla f_c^A = \nabla f_c^B + \varepsilon \boldsymbol{v}^T \nabla^2 f_c^B \tag{38}$$

The estimate of the coupling vector, computed from Eq. (6), is given by

$$\hat{\Gamma}_v^A = \frac{w_2}{w_1} \nabla f_c^A \tag{39}$$

and the angle ξ can be found from the relation

$$\cos \xi = \frac{\Gamma_v^A \bullet \nabla \chi^A}{\|\Gamma_v^A\| \|\nabla \chi^A\|} = \frac{\nabla f_c^A \bullet \nabla \chi^A}{\|\nabla f_c^A\| \|\nabla \chi^A\|} \tag{40}$$

From optimality conditions, it is known that

$$w_a \nabla f_a^B = -w_c \nabla f_c^B \tag{41}$$

$$w_1 \nabla f_a^A = -w_2 \nabla \chi^A \tag{42}$$

Using Eq. (42), it is possible to rewrite Eq. (40) as

$$\cos \xi = \frac{-\nabla f_c^A \bullet \nabla f_a^A}{\|\nabla f_c^A\| \|\nabla f_a^A\|} \tag{43}$$

By following the mathematical procedure detailed in Ref. [19], it can be shown that

$$\cos^2 \xi \left(\nabla^2 f_a^{B^T} \boldsymbol{v} - \frac{1}{\varepsilon} \frac{w_c}{w_a} \nabla f_c^{B^T} \right) \left(\boldsymbol{v}^T \nabla^2 f_c^B \boldsymbol{v} \right) = \left(\nabla^2 f_a^{B^T} \boldsymbol{v} - \frac{1}{\varepsilon} \nabla f_c^{B^T} \right) \left(\boldsymbol{v}^T \nabla^2 f_c^B \boldsymbol{v} \right) \tag{44}$$

Since the functions have been specified as convex, $\boldsymbol{v}^T \nabla^2 f_c^B \boldsymbol{v} \geq 0$ and $\boldsymbol{v}^T \nabla^2 f_c{}^B \boldsymbol{v} \geq 0$. As the value of ϵ increases, it is evident that $\cos^2 \xi$ must decrease, and, therefore, ξ is increasing. Given that ξ has the same monotonicity as ε, the angle ξ is an appropriate measure of the distance between a CPF solution and the unknown Pareto frontier, and the theorem is proven. □

Example. Consider the following problem:

$$\min w_a f_a(\boldsymbol{d}_a) + w_c f_c(\boldsymbol{d}_a, \boldsymbol{d}_c) \tag{45}$$

where

$$f_a = 0.5 d_{a_1}^2 + d_{a_2}^2 - d_{a_1} d_{a_2} - 7 d_{a_1} - 7 d_{a_2} \tag{46}$$

$$f_c = (d_{a_1} - d_{a_2})^2 + \frac{1}{9}(d_{a_1} + d_{a_2} + \boldsymbol{d}_c - 10)^2 + (\boldsymbol{d}_c - 5)^2 \tag{47}$$

A CPF of

$$\chi_1(\boldsymbol{d}_a) = (d_{a_1} - 5)^2 + d_{a_2}^2 - 25 \tag{48}$$

is chosen, and the system is optimized both sequentially and simultaneously. The angle ξ is compared with the distance ϵ to the nearest point on the true Pareto frontier in Fig. 3, and it can be seen that, for this example, this angle is an effective measure of the distance to the frontier. Using this measure, the accuracy of a CPF can be evaluated without knowing the true Pareto frontier.

3.3 Monotonicity of Controller Objective and CPF. A function is said to be coordinate-wise monotonic if it is either always increasing or always decreasing with respect to a given variable, e.g., if the partial derivative of a continuous function does not change sign [28]. Monotonicity analysis is a useful tool in optimization problems. For example, it can be used to determine constraint activity, to study the behavior of composite functions, and to give insight into the tradeoffs present in optimization problems [28]. Here, monotonicity is used to characterize effective CPFs.

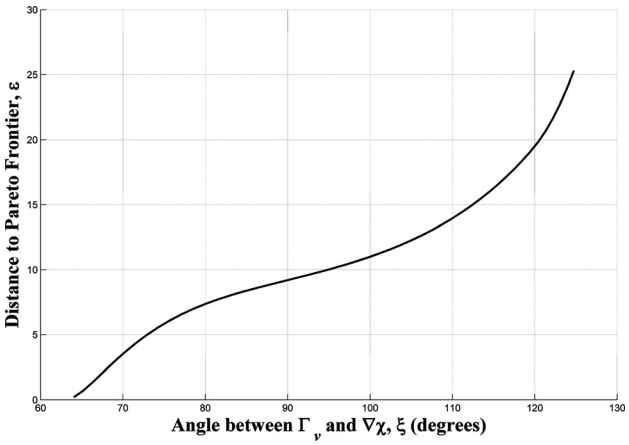

Fig. 3 Comparison of angle ξ and distance ε

If a controller objective $f_c(\boldsymbol{d}_a, \boldsymbol{d}_c)$ is monotonic with respect to an element of $\boldsymbol{d}_a$, then it seems appropriate that $\chi(\boldsymbol{d}_a)$ should have the same monotonicity with respect to that element of $\boldsymbol{d}_a$ in order to effectively model the behavior of f_c.

Theorem 3. *If $f_c(\boldsymbol{d}_a, \boldsymbol{d}_c)$ is monotonic with respect to some element of $\boldsymbol{d}_a$, and that element of $\boldsymbol{d}_a$ does not appear in any active constraint, then a CPF with the same monotonicity will produce solutions closer to the optimum than a CPF with the opposite monotonicity.*

Proof. Assume that, in a codesign problem, the controller objective function $f_c(\boldsymbol{d}_a, \boldsymbol{d}_c)$ is monotonic with respect to the jth component of the n-dimensional vector of artifact design variables $\boldsymbol{d}_a$. Two CPFs will be used to solve this problem, denoted as $\chi_1(\boldsymbol{d}_a)$ and $\chi_2(\boldsymbol{d}_a)$. The two CPFs are selected such that they have opposite monotonicity with respect to the jth component of $\boldsymbol{d}_a$, i.e., one CPF is increasing with respect to d_{a_j}, while the other is decreasing with respect to d_{a_j} [28]. Mathematically, this can be stated as follows:

$$\frac{\partial \chi_1}{\partial d_{a_i}} = \frac{\partial \chi_2}{\partial d_{a_i}} \ \forall \ \{i : i \neq j, 1 \leq i \leq n\} \tag{49}$$

$$\frac{\partial \chi_1}{\partial d_{a_j}} = -\frac{\partial \chi_2}{\partial d_{a_j}} \tag{50}$$

$$\operatorname{sgn}\left(\frac{\partial \chi_1}{\partial d_{a_j}} \right) = \operatorname{sgn}\left(\frac{\partial f_c}{\partial d_{a_j}} \right) \tag{51}$$

Let the point A in the $\boldsymbol{d}_a$-space be a solution to the CPF problem using $\chi_1(\boldsymbol{d}_a)$, and let point B in the $\boldsymbol{d}_a$-space be the Pareto optimal solution to the codesign problem that is nearest to point A. Assume that, at point B, d_{a_j} does not appear in any active controller constraints $\boldsymbol{g}_c(\boldsymbol{d}_a, \boldsymbol{d}_c)$ or $\boldsymbol{h}_c(\boldsymbol{d}_a, \boldsymbol{d}_c)$. Choose point C such that it is a solution to the CPF problem using $\chi_2(\boldsymbol{d}_a)$ and such that point B is the Pareto-optimal point nearest to it, as shown in Fig. 4.

If the distances from point B to points A and C, denoted as ε^A and ε^C, respectively, are sufficiently small, then the functions f_c, χ_1, and χ_2 can each be represented by first-order Taylor series approximations. Expanding about B,

$$f_c^A = f_c^B + \varepsilon^A \nabla f_c^B \boldsymbol{v}_1 \tag{52}$$

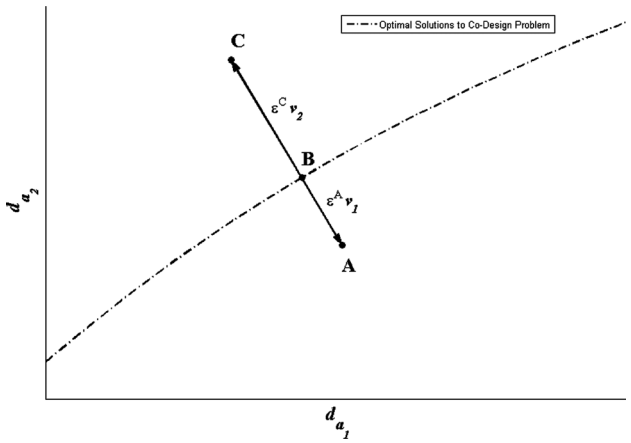

Fig. 4 Pareto-optimal Point B and CPF Points A and C

$$f_c^C = f_c^B + \varepsilon^C \nabla f_c^B \boldsymbol{v}_2 \tag{53}$$

$$\chi_1^A = \chi_1^B + \varepsilon^A \nabla \chi_1^B \boldsymbol{v}_1 \tag{54}$$

$$\chi_2^C = \chi_2^B + \varepsilon^C \nabla \chi_2^B \boldsymbol{v}_1 \tag{55}$$

where $\boldsymbol{v}_1$ and $\boldsymbol{v}_2$ are unit vectors such that $\boldsymbol{v}_2 = \pm \boldsymbol{v}_1$.

By taking gradients of Eqs. (52) and (53), it can be stated that

$$\nabla f_c^A = \nabla f_c^B \tag{56}$$

$$\nabla f_c^C = \nabla f_c^B \tag{57}$$

The coupling vector estimates at A and C are given by

$$\widehat{\Gamma}_v^A = \frac{w_2^A}{w_1^A} \nabla f_c^A \tag{58}$$

$$\widehat{\Gamma}_v^C = \frac{w_2^C}{w_1^C} \nabla f_c^A \tag{59}$$

where w_1^A and w_2^A are the weights which produce point A, and w_1^C and w_2^C are the weights which produce point C. Substituting Eqs. (56) and (57) into Eqs. (58) and (59)

$$\widehat{\Gamma}_v^A = \frac{w_2^A}{w_1^A} \nabla f_c^B \tag{60}$$

$$\widehat{\Gamma}_v^C = \frac{w_2^C}{w_1^C} \nabla f_c^B \tag{61}$$

The gradients $\nabla \chi_1^A$ and $\nabla \chi_2^C$ are given by the relations

$$\nabla \chi_1^A = \nabla \chi_1^B \tag{62}$$

$$\nabla \chi_2^C = \nabla \chi_2^B \tag{63}$$

Using Eqs. (58)–(63), ξ can be found for A and C

$$\cos \xi^A = \frac{\widehat{\Gamma}_v^A \bullet \nabla \chi_1^A}{\left\| \widehat{\Gamma}_v^A \right\| \| \nabla \chi_1^A \|} \tag{64}$$

$$\cos \xi^C = \frac{\widehat{\Gamma}_v^C \bullet \nabla \chi_2^A}{\left\| \widehat{\Gamma}_v^C \right\| \| \nabla \chi_2^C \|} \tag{65}$$

Substituting into Eqs. (64) and (65), it is possible to relate ξ^A and ξ^C, as shown in Ref. [19], and to show that $\cos \xi^A > \cos \xi^C$, leading to the conclusion that $\xi^A < \xi^C$. Therefore, from Theorem 2, it can be stated that $\chi_1(\boldsymbol{d}_a)$ will produce solutions closer to the Pareto optimal points than $\chi_2(\boldsymbol{d}_a)$ will. Since $\chi_1(\boldsymbol{d}_a)$ shares the same monotonicity as $f_c(\boldsymbol{d}_a, \boldsymbol{d}_c)$, the theorem is proven. □

Example. Consider the following problem:

$$\min w_a f_a(\boldsymbol{d}_a) + w_c f_c(\boldsymbol{d}_a, \boldsymbol{d}_c) \tag{66}$$

$$\text{subject to } g_a(\boldsymbol{d}_a) = 10 - d_{a_1} - d_{a_2} \le 0 \tag{67}$$

$$\boldsymbol{g}_c(\boldsymbol{d}_a, \boldsymbol{d}_c) = \left(d_{a_2} - \frac{\boldsymbol{d}_c}{2} \right)^2 - 25 \le 0 \tag{68}$$

where

$$f_a = 0.5 d_{a_1}^2 + d_{a_2}^2 - d_{a_1} d_{a_2} - 7 d_{a_1} - 7 d_{a_2} \tag{69}$$

$$f_c = d_{a_1} + d_{a_2} - \boldsymbol{d}_c \tag{70}$$

and $\boldsymbol{d}_a = \{ \boldsymbol{d}_a : \boldsymbol{d}_a \ge \boldsymbol{0} \}$.

A CPF of

$$\chi_1(\boldsymbol{d}_a) = d_{a_1} + 0.25 d_{a_2}^{0.5} \tag{71}$$

is chosen. It is evident that f_c and χ are both monotonically increasing with respect to d_{a_1} and d_{a_2}. Solving both the simultaneous optimization and the CPF problem, it can be seen in Fig. 5 that the CPF solution models the tradeoff between f_a and f_c, though imperfectly.

In contrast, consider a CPF of

$$\chi_2(\boldsymbol{d}_a) = -d_{a_1} + 0.25 d_{a_2}^{0.5} \tag{72}$$

In this case, the monotonicities of χ and f_c with respect to d_{a_1} do not match. Solving the new CPF problem, it can be seen in Fig. 5 that this CPF does not model the tradeoff between f_a and f_c.

3.4 Locations of Unconstrained Minima of f_c and χ. In Sec. 3.3, f_c was assumed to be monotonic with respect to some element of $\boldsymbol{d}_a$. Here, the case where f_c is not monotonic, but rather has an unconstrained minimum, is considered. Intuitively, it seems to be likely that the values taken by $\boldsymbol{d}_a$ at the minimum of f_c should also minimize χ, and that a CPF will become less effective if the minimum of χ is farther from the minimum of f_c in the $\boldsymbol{d}_a$-space. This can be proven for an unconstrained problem, and it is conjectured that it will also be true for constrained problems.

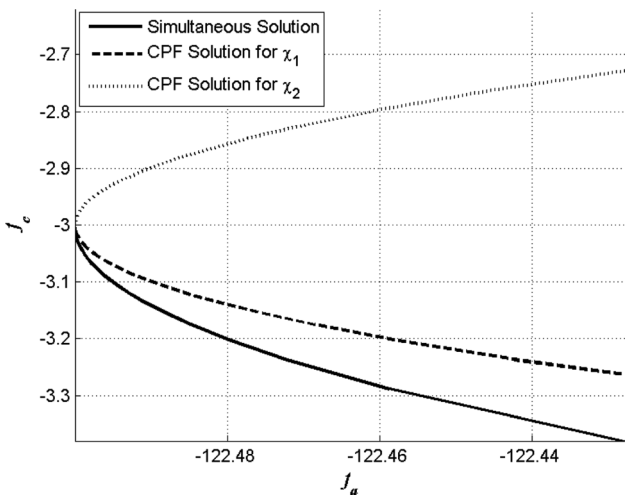

Fig. 5 Comparison of simultaneous and CPF solutions for appropriate and inappropriate monotonicity

Theorem 4. *Assume that $f_c(\boldsymbol{d}_a, \boldsymbol{d}_c)$ has an unconstrained minimum, and that $\chi(d_a)$ is chosen such that it has an unconstrained minimum. Then, the distance between a CPF point and the Pareto frontier will increase as the distance increases between the minima of f_c and χ.*

Proof. Assume that in a codesign problem the control objective function $f_c(\boldsymbol{d}_a, \boldsymbol{d}_c)$ has an unconstrained minimum in the $\boldsymbol{d}_a$-space, denoted as point D. The CPF $\chi(\boldsymbol{d}_a)$ is chosen such that it has an unconstrained minimum in the $\boldsymbol{d}_a$-space. The minimum of $\chi(\boldsymbol{d}_a)$, denoted as point C, is located at a distance δ from point D, as shown in Fig. 6.

Let point A be a solution to the CPF problem using $\chi(\boldsymbol{d}_a)$. The distance from point D to point A is denoted as σ, and the distance from point C to point A is denoted as β. The vectors $\boldsymbol{n}$, $\boldsymbol{r}$, and $\boldsymbol{s}$ in Fig. 6 are unit vectors.

The function f_c evaluated at point A shall be represented by a second-order Taylor series expansion about its minimum, point D, as follows:

$$f_c^A = f_c^D + \frac{1}{2}\sigma^2 \boldsymbol{s}^T \nabla^2 f_c^D \boldsymbol{s} \tag{73}$$

The function χ evaluated at point A shall be represented by a second-order Taylor series expansion about its minimum, point C, as follows:

$$\chi^A = \chi^C + \frac{1}{2}\beta^2 \boldsymbol{r}^T \nabla^2 \chi^C \boldsymbol{r} \tag{74}$$

It is then possible to find the gradients of f_c and χ, evaluated at point A, in the $\boldsymbol{d}_a$-space.

$$\nabla f_c^A = \sigma \boldsymbol{s}^T \nabla^2 f_c^D \tag{75}$$

$$\nabla \chi^A = \beta \boldsymbol{r}^T \nabla^2 \chi^C \tag{76}$$

The unit vector $\boldsymbol{r}$ can be expressed as $\boldsymbol{r} = \frac{1}{\beta}(\sigma \boldsymbol{s} - \delta \boldsymbol{n})$, and, therefore, Eq. (76) can be rewritten as

$$\nabla \chi^A = (\sigma \boldsymbol{s} - \delta \boldsymbol{n})^T \nabla^2 \chi^C \tag{77}$$

From Eq. (40), it is known that

$$\cos \xi^A = \frac{\nabla \chi^A \bullet \nabla f_c^A}{\|\nabla \chi^A\| \|\nabla f_c^A\|} \tag{78}$$

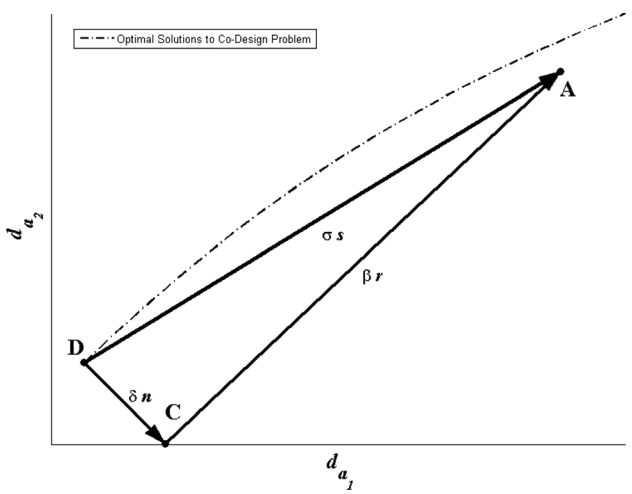

Fig. 6 Unconstrained minima of f_c and χ

The unit vector $\boldsymbol{s}$ can be expressed in terms of the unit vector $\boldsymbol{n}$ by means of a rotation matrix, R, as $\boldsymbol{s} = \boldsymbol{R}\boldsymbol{n}$; substituting this relation and Eqs. (75) and (76). Following the mathematical steps given in Ref. [19], it is possible to establish the monotonicity of $\cos \xi^A$ with respect to δ. It can be shown that, regardless of the value of δ, an increase in δ will always result in a decrease in $\cos \xi^A$; thus, we see that an increase in the distance δ between the minima of f_c and χ will result in an increase in the angle ξ^A. From Theorem 2, it can be stated that an increase in δ will result in CPF solutions that are farther from the Pareto-optimal solutions to the codesign problem, and thus, the theorem is proven. □

Example. Consider the following problem:

$$\min w_a f_a(\boldsymbol{d}_a) + w_c f_c(\boldsymbol{d}_a, \boldsymbol{d}_c) \tag{79}$$

$$\text{subject to} \quad g_a(\boldsymbol{d}_a) = 4d_{a_1}^2 + d_{a_2}^2 - 900 \le 0 \tag{80}$$

$$\boldsymbol{g}_c(\boldsymbol{d}_a, \boldsymbol{d}_c) = \frac{1}{50} d_{a_1}^2 + \frac{1}{5} d_{a_2}^2 - 48 \le 0 \tag{81}$$

where

$$f_a = 0.5 d_{a_1}^2 + d_{a_2}^2 - d_{a_1} d_{a_2} - 7 d_{a_1} - 7 d_{a_2} \tag{82}$$

$$f_c = (d_{a_1} - d_{a_2})^2 + \frac{1}{9}(d_{a_1} + d_{a_2} + \boldsymbol{d}_c - 10)^2 + (\boldsymbol{d}_c - 5)^2 \tag{83}$$

This problem is solved twice, with two different CPFs, which are then compared

$$\chi_1(\boldsymbol{d}_a) = (d_{a_1} - 5)^2 + d_{a_2}^2 - 25 \tag{84}$$

$$\chi_2(\boldsymbol{d}_a) = (d_{a_1} - 1)^2 + (d_{a_2} + 10)^2 - 10 \tag{85}$$

The unconstrained minima of the functions f_a, f_c, χ_1, and χ_2 are given in Table 1. The minimum of χ_1 is located at a distance of 3.54 from the minimum of f_c, significantly closer than the minimum of χ_2, which is located at a distance of 12.59 from the minimum of f_c. The solutions found by solving the two CPF sequential problems are shown in Fig. 7. It can be seen that χ_1, which obtains its minimum closer to that of f_c than does χ_2, produces a closer match to the simultaneous solution than χ_2.

It is important to note that, in the case of Theorem 1, no assumptions were made about the functional forms of f_a, f_c, or χ. For Theorems 2 through 4, the functions were assumed to be convex in the region of interest. This assumption allowed higher-order terms to be neglected without changing the sign of the Taylor series expansion. If a function was nonconvex, then the results of Theorems 2 through 4 would not necessarily be applicable.

4 Control Proxy Functions for Specific Codesign Problem Formulations

In Sec. 3, the characteristics of effective CPFs have been shown. The four theorems presented were based purely on the mathematics of the functions involved in the problem, with no consideration for what they might physically represent or what specific problems could be formulated. Here, specific codesign problem formulations are considered, and the types of CPFs that may apply to those problems are studied.

Previous work has shown that, in some cases, the natural frequency of a system can be used as an effective proxy for that

Table 1 Comparison of minima of objective functions and control proxy functions

	f_a	f_c	χ_1	χ_2
d_{a_1}	21	2.5	5	1
d_{a_2}	14	2.5	0	−10

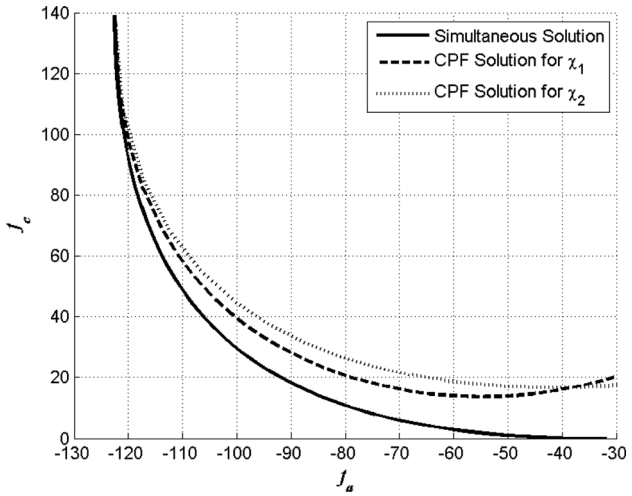

Fig. 7 Comparison of simultaneous and CPF solutions for two choices of CPF

system's ease of control (e.g., Refs. [29–33]), and the natural frequency has been successfully used in many structural problems, in which minimizing vibration is critical. Furthermore, it has been demonstrated that, in certain cases, a CPF based on natural frequency is guaranteed to produce the system-optimal results [34]. Such a CPF is not always effective, however; in particular, when the system's response to a forcing function is sensitive to the artifact design variables, a CPF based on natural frequency will not be effective since it does not capture this behavior. Therefore, additional CPFs are necessary to cover a wide range of problems of interest. Here, the controllability Grammian matrix, $\boldsymbol{W}_c$, will be considered as the basis for a CPF. Previous work has shown that, for some problem formulations, there is a relationship between $\boldsymbol{W}_c$ and the coupling vector $\boldsymbol{\Gamma}_v$ [35]. Since there is also a relationship between $\boldsymbol{\Gamma}_v$ and an effective CPF, this suggests that a CPF based on $\boldsymbol{W}_c$ will be effective for some problems.

This section will examine situations in which a CPF based on either the time-dependent controllability Grammian matrix, $\boldsymbol{W}_c(t_f)$ or the steady-state controllability Grammian matrix, $\boldsymbol{W}_c{}^{\infty}$, is perfect. In all cases, it is assumed that the codesign problem is formulated as in Eqs. (1)–(5), and that the system dynamics are linear and can be described in state-space form, i.e., $\dot{\boldsymbol{x}} = \boldsymbol{A}\boldsymbol{x} + \boldsymbol{B}u$, where $\boldsymbol{A}$ describes the system's free response, $\boldsymbol{B}$ characterizes the system's response to a forcing function, u is the control input, and $\boldsymbol{x}$ is the vector of system states.

4.1 Control Proxy Function for the Case of Control Effort as Objective. Consider the case in which the control objective is to minimize control effort, defined as

$$f_c = \int_0^{t_f} (u(t))^2 dt \tag{86}$$

It is known from control theory that there exists a minimum possible value for the control effort, regardless of the controller architecture chosen, and that this limit is dependent on the controllability Grammian matrix, $\boldsymbol{W}_c$ [36]. Therefore, if an optimal controller is chosen, then the control objective function f_c will be given by

$$f_c = x_f^T \boldsymbol{W}_c^{-1} x_f \tag{87}$$

This expression for f_c depends only on $\boldsymbol{d}_a$ and thus could serve as a CPF. It has been shown that the coupling vector $\boldsymbol{\Gamma}_v$ is related to $\boldsymbol{W}_c$ [35], and for the control objective in Eq. (87) is given by

$$\Gamma_v = \frac{w_c}{w_a}\begin{bmatrix} \boldsymbol{x}_f^T \dfrac{\partial \boldsymbol{W}_c^{-1}}{\partial d_{a_1}} \boldsymbol{x}_f + 2\boldsymbol{x}_f^T \boldsymbol{W}_c^{-1} \dfrac{\partial \boldsymbol{x}_f}{\partial d_{a_1}} \\ \boldsymbol{x}_f^T \dfrac{\partial \boldsymbol{W}_c^{-1}}{\partial d_{a_2}} \boldsymbol{x}_f + 2\boldsymbol{x}_f^T \boldsymbol{W}_c^{-1} \dfrac{\partial \boldsymbol{x}_f}{\partial d_{a_2}} \\ \vdots \\ \boldsymbol{x}_f^T \dfrac{\partial \boldsymbol{W}_c^{-1}}{\partial d_{a_n}} \boldsymbol{x}_f + 2\boldsymbol{x}_f^T \boldsymbol{W}_c^{-1} \dfrac{\partial \boldsymbol{x}_f}{\partial d_{a_n}} \end{bmatrix}^T \tag{88}$$

For $\chi(\boldsymbol{d}_a) = \boldsymbol{x}_f^T \boldsymbol{W}_c{}^{-1} x_f$, $\Gamma_v = \frac{w_c}{w_a}\nabla\chi$, and thus, the CPF is perfect.

There are situations, however, when a simpler CPF would suffice. Consider the case where the final state of the system, $\boldsymbol{x}_f$, is a parameter. One might expect that when this is the case, a CPF based only on $\boldsymbol{W}_c$ may be effective, and in some situations this is true, as shown below.

Consider a situation in which the parameter $\boldsymbol{x}_f$ has as its only nonzero component the jth element, i.e., $x_{f_j} \neq 0$, $x_{f_q} = 0 \; \forall \; q \neq j$; this situation corresponds to problems, e.g., in which a system is to be moved to a final location where it is at rest. A CPF of

$$\chi = \boldsymbol{W}_{c_{jj}}^{-1}(t_f) = \frac{\boldsymbol{W}_{c_{jj}}^*(t_f)}{\det(\boldsymbol{W}_c)} \tag{89}$$

is chosen, where $\boldsymbol{W}_c^*(t_f)$ is the adjoint matrix of $\boldsymbol{W}_c(t_f)$, and $\boldsymbol{W}_{c_{jj}}^*(t_f)$ is the (jj)th element of $\boldsymbol{W}_c^*(t_f)$. Note that, if the (jj)th element of $\boldsymbol{W}_c{}^*(t_f)$ is not a function of $\boldsymbol{d}_a$, then this is equivalent to maximizing the determinant of $\boldsymbol{W}_c(t_f)$. It will be shown here that this is a perfect CPF.

The gradient of Eq. (89) is given by

$$\nabla\chi = \left[\frac{\partial \boldsymbol{W}_{c_{jj}}^{-1}(t_f)}{\partial d_{a_1}}, \frac{\partial \boldsymbol{W}_{c_{jj}}^{-1}(t_f)}{\partial d_{a_2}}, \ldots, \frac{\partial \boldsymbol{W}_{c_{jj}}^{-1}(t_f)}{\partial d_{a_n}}\right] \tag{90}$$

The coupling vector $\boldsymbol{\Gamma}_v$ is found from Eq. (88)

$$\Gamma_v = \frac{w_c}{w_a}\left[x_{f_j}^2 \frac{\partial \boldsymbol{W}_{c_{jj}}^{-1}(t_f)}{\partial d_{a_1}}, \quad \ldots, \quad x_{f_j}^2 \frac{\partial \boldsymbol{W}_{c_{jj}}^{-1}(t_f)}{\partial d_{a_n}}\right] \tag{91}$$

which can be rewritten as

$$\Gamma_v = \frac{w_c}{w_a} x_{f_j}^2 \nabla\chi \tag{92}$$

Thus, as stated, Eq. (89) will be a perfect CPF for this situation.

It has been shown that the coupling vector is related to the controllability Grammian matrix for the case where the control objective function is the final time and a constraint on control effort is active [35]. The coupling vector for that problem formulation was found to be parallel to the coupling vector found when the control objective function is control effort. Therefore, it can then be seen that the CPF developed above will also apply to such problems.

4.2 Control Proxy Function for the Case of Linear Quadratic Regulator (LQR): In the LQR problem, a cost function J is to be minimized, where J is given in Eq. (93) below and the weighting matrices $\boldsymbol{Q}$ and $\boldsymbol{R}$ denote the relative cost of errors and of control, respectively, [36]

$$J = \int_0^{\infty} \left(\boldsymbol{x}(t)^T \boldsymbol{Q}\boldsymbol{x}(t) + \boldsymbol{u}(t)^T \boldsymbol{R}\boldsymbol{u}(t)\right) dt \tag{93}$$

The coupling vector for the LQR problem can be related to the controllability Grammian for a specific choice of the state weighting matrix $\boldsymbol{Q} = \gamma \boldsymbol{B}\boldsymbol{B}^T$ [35], where γ is a positive scalar value. In the most general, such LQR case, the initial state $\boldsymbol{x}_0$, $\boldsymbol{W}_c{}^{\infty}$, and $\boldsymbol{A}$ all depend on $\boldsymbol{d}_a$, and a perfect CPF would take the form of

$$\chi(\boldsymbol{d}_a) = \boldsymbol{x}_0^T \boldsymbol{A}^{-T} \boldsymbol{A} \boldsymbol{W}_c^{\infty} \boldsymbol{x}_0 \tag{94}$$

As in previous cases, however, there are special circumstances where a simpler CPF may be chosen. This may be desirable in

large problems where computational effort must be reduced. Consider the situation where the matrix $\boldsymbol{A}$ is not a function of $\boldsymbol{d}_a$. Such a situation, while not common, may occur when considering the problem of locating an actuator for canceling vibrations. If the actuator mass is small, its position will not affect the free response of the system; however, it will affect the forced response of the system. Furthermore, assume that the initial state $\boldsymbol{x_0}$ is a parameter with exactly one nonzero component, i.e., $x_{0_j} \neq 0$, $x_{0_q} = 0 \; \forall \; q \neq j, 0 \leq q \leq p$, and the matrix $\boldsymbol{W}_c{}^{\infty}$ is diagonal, which will be the case when a balanced realization is utilized [36].

For the system described above, select the CPF

$$\chi(\boldsymbol{d}_a) = \boldsymbol{W}^{\infty}_{c_{jj}} \tag{95}$$

Its gradient is

$$\nabla\chi = \left[\frac{\partial \boldsymbol{W}^{\infty}_{c_{jj}}}{\partial d_{a_1}}, \quad \frac{\partial \boldsymbol{W}^{\infty}_{c_{jj}}}{\partial d_{a_2}}, \quad \ldots, \frac{\partial \boldsymbol{W}^{\infty}_{c_{jj}}}{\partial d_{a_n}}\right] \tag{96}$$

and the coupling vector is given by the relation [35]

$$\Gamma_v = \frac{w_c}{w_a}\gamma \begin{bmatrix} \dfrac{1}{\det \boldsymbol{A}} x_{0_j}^2 A_{jj}^2 \dfrac{\partial \boldsymbol{W}^{\infty}_{c_{jj}}}{\partial d_{a_1}} \\ \dfrac{1}{\det \boldsymbol{A}} x_{0_j}^2 A_{jj}^2 \dfrac{\partial \boldsymbol{W}^{\infty}_{c_{jj}}}{\partial d_{a_2}} \\ \vdots \\ \dfrac{1}{\det \boldsymbol{A}} x_{0_j}^2 A_{jj}^2 \dfrac{\partial \boldsymbol{W}^{\infty}_{c_{jj}}}{\partial d_{a_n}} \end{bmatrix}^T \tag{97}$$

This leads to the relation

$$\Gamma_v = \frac{w_c}{w_a}\frac{\gamma}{\det \boldsymbol{A}} x_{0_j}^2 A_{jj}^2 \nabla\chi \tag{98}$$

and therefore, the CPF is perfect for this problem.

In this section, it has been shown that a CPF based on the controllability Grammian matrix, $\boldsymbol{W}_c(t_f)$, can be effective for many problems, in which either f_c or an active constraint is dependent on control effort. This includes some problems in which the control objective, f_c, is the response time of the system. For the specific problem formulations investigated here, a perfect CPF can be formulated based on either the time-dependent or the steady-state controllability Grammian matrix. As previously stated, these problem formulations are not exhaustive. It is anticipated that future work will show that a CPF based on the controllability Grammian matrix will be effective for additional codesign problem formulations, particularly, those in which the objective function or constraints are dependent on control effort.

However, it may not always be possible to formulate a perfect CPF based on the control Grammian. For example, consider the case where f_c is the maximum control signal, rather than control effort. A control signal with a high peak that quickly decays may result in a lower control effort than a signal with a lower peak that does not decay as quickly. The relationship between the maximum control signal and control effort, and the choice of an appropriate CPF for problems in which the control objective, f_c, is based on the maximum control signal, requires further investigation. It is expected that a CPF based on the controllability Grammian will produce results that are near-optimal for a variety of problems, since it provides a measure of how easily a system is controlled.

5 MEMS Actuator and Controller Optimization

The MEMS actuator considered in this case study was originally designed by Tung and Kurabayashi [37] and is shown in Fig. 8. This actuator has been designed to produce out-of-plane displacements and could be useful in a variety of applications, such as a confocal scanning microscope [37]. The actuator utilizes four electrostatic comb-drive actuators to produce this out-of-plane displacement. The actuator can be used to produce an angular deflection of the platform as well, but, here, only the vertical displacement of the platform is considered. In order to produce this displacement, each of the four comb drives is excited with a voltage, V, resulting in horizontal (in-plane) movement (ΔX) of the silicon shuttles. The microhinges on the polydimethyl siloxane (PDMS) platform bend, and the platform moves vertically, or out-of-plane (ΔZ). The amount of movement resulting from the comb drives' actuation depends on both the applied voltage, V, and the physical dimensions of the actuator. Changing the actuator's dimensions results in a different output displacement for the same applied voltage.

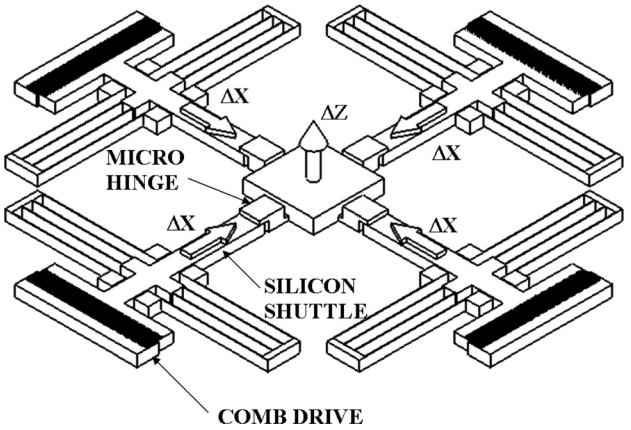

Fig. 8 MEMS actuator configuration

The displacement of the actuator, ΔZ, is given by the equation

$$\Delta Z = (h_1 + h_2)(1 - \cos\Delta\theta) + (t + p)\sin\Delta\theta \tag{99}$$

where p, t, h_1, and h_2 are the hinge dimensions shown in Fig. 9, and $\Delta\theta$ is the angular displacement of the hinge.

The angular displacement $\Delta\theta$ can be found from the differential equation

$$M\Delta\ddot{\theta} + C\Delta\dot{\theta} + K\Delta\theta = A(\Delta\theta)V^2 \tag{100}$$

where M, C, K, and $A(\Delta\theta)$ are functions of the actuator geometry. Derivations, and the equations for the various masses and stiffnesses of the system components, are given in Ref. [37] and reproduced in Ref. [19]. Alternatively, the system dynamics may be written in state-space form, with $\boldsymbol{x} = \left[\Delta\theta \;\; \Delta\dot{\theta}\right]^T$, as

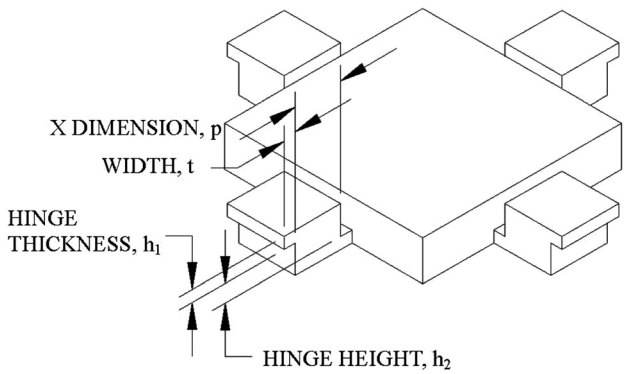

Fig. 9 Microhinge structure

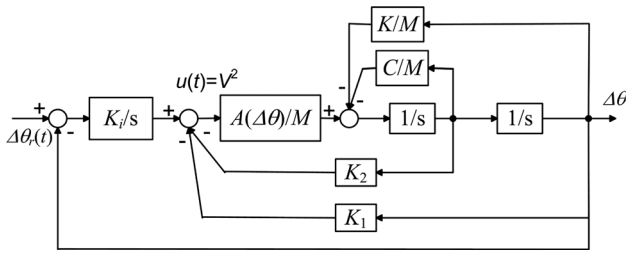

Fig. 10 Control architecture and system dynamics

$$\begin{bmatrix} \Delta\dot{\theta} \\ \Delta\ddot{\theta} \end{bmatrix} = \begin{bmatrix} 0 & 1 \\ -K/M & -C/M \end{bmatrix} \begin{bmatrix} \Delta\theta \\ \Delta\dot{\theta} \end{bmatrix} + \begin{bmatrix} 0 \\ A(\Delta\theta)/M \end{bmatrix} V^2 \quad (101)$$

An integral controller with state feedback is applied to the system, as shown in Fig. 10. It is assumed that the angle $\Delta\theta$ and the angular velocity $\Delta\dot{\theta}$ can be measured, and that the angle $\Delta\theta$ is to be controlled. The dynamics of the closed-loop system can then be written as

$$M\Delta\ddot{\theta} + (C + K_2 A(\Delta\theta))\Delta\dot{\theta} + (K + K_1 A(\Delta\theta))\Delta\theta - K_i A(\Delta\theta)\int_0^t (\Delta\theta_r - \Delta\theta)d\tau = 0 \quad (102)$$

Note that the controller output is $u = V^2$, and that the coefficient A in Eq. (100) is a function of $\Delta\theta$. Thus, the resulting controller design problem is nonlinear.

5.1 Optimization Problem Formulation. The artifact objective is to maximize the final displacement of the actuator, ΔZ_f, at a given time t_f, where ΔZ_f is the peak displacement and is 5% higher than the steady-state displacement, ΔZ_{ss}, see Eq. (103). This objective function is chosen with the assumption that, while the final position is important, there may be times in which the actuator's steady-state displacement is important, and, therefore, the relationship between the two is relevant to the problem. Artifact constraints based on manufacturability, kinematics, mechanical and electrical stability, and stress, are given in Eqs. (105)–(110). The artifact design variables, $\boldsymbol{d}_a$, are p, t, and the shuttle length l_1, with the bounds in Eqs. (111)–(113). The control objective is to minimize the actuation control effort, see Eq. (104). The control design variables are the gains K_1, K_2, and K_i. There are no control constraints. These variables are summarized in Table 2.

$$f_a = -\Delta Z_f = -1.05\Delta Z_{ss} \quad (103)$$

$$f_c = \int_0^{t_f} (u(t))^2 dt = \int_0^{t_f} (V(t))^4 dt \quad (104)$$

$$g_{a_1} = t - 5h_1 \le 0 \quad (105)$$

$$g_{a_2} = 910 - l_1 - \frac{l_p}{2} - 2t + \frac{\Delta X_{ss}}{2} \le 0 \quad (106)$$

Table 2 Design and control variables for MEMS actuator optimization

$\boldsymbol{d}_a$	p	Microhinge length
	t	Microhinge width
	l_1	Shuttle length
$\boldsymbol{d}_c$	K_1	Controller gain for $\Delta\theta$
	K_2	Controller gain for $\Delta\dot{\theta}$
	K_i	Integral controller gain

$$g_{a_3} = \frac{n\varepsilon_o(h_1 + h_2)V_{ss}^2}{d} - \frac{k_b\pi^2 E_{PDMS} w(2h_1 + h_2)^3}{12p^2} \le 0 \quad (107)$$

$$g_{a_4} = \Delta X_{ss} - \left(\frac{l_{Si}}{\sqrt{2}} - \frac{l_{fo}}{2}\right) \le 0 \quad (108)$$

$$g_{a_5} = \frac{E_{PDMS} h_1 \Delta\theta_{ss}}{2p} - \sigma_{PDMS_{max}} \le 0 \quad (109)$$

$$g_{a_6} = \frac{3\Delta X_{ss} E_{Si} b}{4l_{Si}^2} - \sigma_{Si_{max}} \le 0 \quad (110)$$

$$1\ \mu\text{m} \le p \le 1000\ \mu\text{m} \quad (111)$$

$$1\ \mu\text{m} \le t \le 1000\ \mu\text{m} \quad (112)$$

$$100\ \mu\text{m} \le l_1 \le 1000\ \mu\text{m} \quad (113)$$

Here, $n = 50$ is the number of fingers in the comb drive, $\varepsilon_o = 8.854e-12$ F/m is the permittivity of vacuum, $d = 3$ μm is the width of a finger, $b = 3$ μm is the thickness of the silicon leaf spring, $w = 100$ μm is the depth of the micro-hinge, $l_p = 350$ μm is the length of the platform, $k_b = 0.25$ is the beam end condition coefficient, $E_{PDMS} = 750$ kPa is Young's modulus for PDMS, $l_{Si} = 500$ μm is the length of the silicon springs, $l_{fo} = 50$ μm is the initial finger engagement, $E_{Si} = 190$ GPa is Young's modulus for silicon, and $\sigma_{PDMS_{max}} = 2.24$MPa and $\sigma_{Si_{max}} = 1.5$GPa are maximum allowable stresses in PDMS and silicon, respectively. The steady-state actuator displacement, ΔZ_{ss}, can be found from Eq. (99). The final time is a parameter, $t_f = 0.25$ ms.

It is possible to define a variety of possible measures of "ease of control," which might serve as a CPF. Such measures could be based on natural frequency, the controllability Grammian matrix, the reference signal used to produce the displacement, or a variety of other measures. The choice of which possible CPF to use is based on knowledge of the control objective function and on the fundamental control limitations present in the system. In this case, the CPF problem to be solved is

$$\min_{p,t,l_1} w_1 f_a + w_2 \chi = w_1 f_a + w_2 \frac{\Delta Z_f^2 W_{c_{22}}(t_f)}{\det(\boldsymbol{W}_c(t_f))} \quad (114)$$

subject to the constraints in Eqs. (105)–(110); followed by

$$\min_{K_1,K_2,K_i} E = \int_0^{t_f} (V(t))^4 dt \quad (115)$$

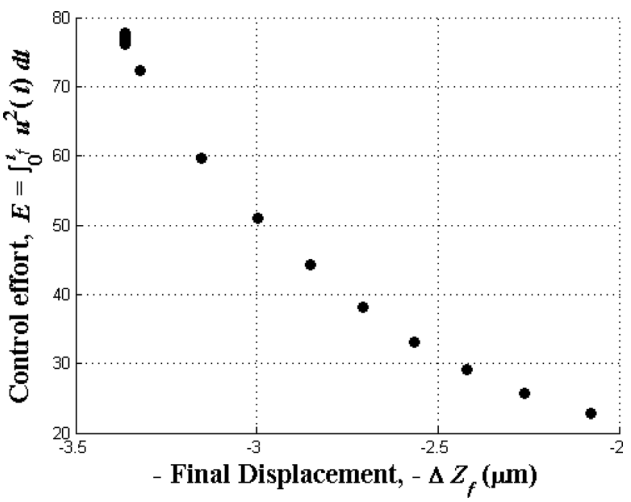

Fig. 11 CPF points for optimization of MEMS actuator

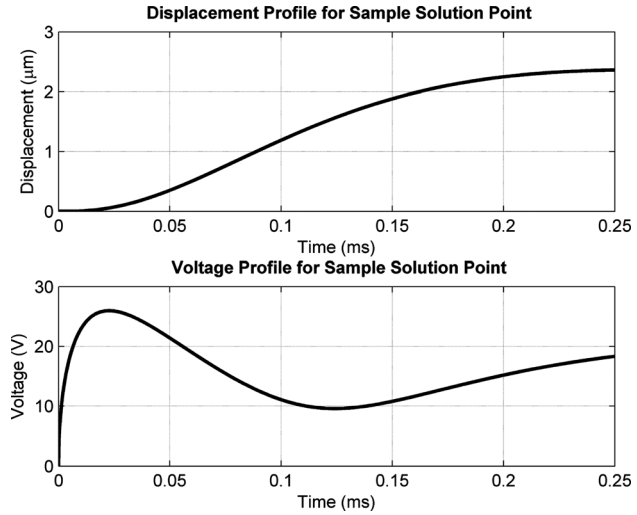

Fig. 12 Displacement and voltage profile for sample MEMS actuator design

Optimal values of $-\Delta Z_f$ and E are shown in Fig. 11, with simulation results for one point shown in Fig. 12. Once a design is selected, since the closed-loop system is nonlinear, we can conduct linearization and a local stability analysis to ensure closed-loop stability. At each of the points shown, the angle ξ is calculated in order to determine whether the point is optimal or near-optimal. For each point, $\xi = 0$, indicating that the CPF points are Pareto optimal. However, the CPF points require less computational effort. Using MATLAB, a typical CPF point required 7 s of computational time, while a simultaneous solution for that point required 577 s of computational time.

The accuracy of this CPF can be ascertained by examining f_c, whose value is found from Eq. (87), where $x_f = [\Delta Z_f, \quad 0]^T$. Since for an optimal controller, $f_c = \chi$, the tradeoff between displacement and control effort can be evaluated using χ, prior to the formulation of the control optimization problem.

6 Concluding Remarks

A new sequential method for optimization of codesign problems was introduced using a CPF. The method provides solutions that are identical or close to the Pareto optimal solutions to the codesign problem, while the decomposed problem is easier to solve sequentially. The method's effectiveness depends on the choice of CPF. Guidelines for choosing a CPF and a metric to evaluate the closeness of the solutions were developed and illustrated with examples. While the method is presented under some assumptions, such as the presence of unidirectional coupling, these assumptions are not unique to the codesign problem. Any bi-objective problem exhibiting unidirectional coupling could be successfully solved for optimal or near-optimal solutions with an appropriate proxy function that satisfies conditions such as those set forth in this work.

Some limitations were specified in the development of the theory. A particularly limiting assumption is that no constraints be active in certain cases. It is expected that the unconstrained case provides a bound, and that the performance of a CPF for a constrained problem will be no worse than the performance of that CPF if the constraints were not present. Proof of this conjecture should be a subject of future work. A further limitation is that the assumption was made that the functional form of the control objective is known, e.g., that f_c can be expressed in terms of $\boldsymbol{d}_a$ and $\boldsymbol{d}_c$. In the case of so-called "black-box" controllers, this is not true. In these cases, it may be possible to formulate a CPF based on knowledge of the underlying physics that limits controller performance. If this approach is not possible, then an experimental approach could be taken, in which a design of experiments is used to empirically construct a CPF. Such problems are of interest, and should be a subject of future work.

One can discover CPFs for specific codesign problem formulations. Examples are CPFs based on natural frequency [34] and on the controllability Grammian matrix presented here. It is anticipated that a variety of CPFs could be formulated for a wide range of problems, motivated by the work presented.

Acknowledgment

This work was partially supported by NSF Grant No. 0625060 and by the Automotive Research Center (ARC). This support is gratefully acknowledged.

Nomenclature

$\boldsymbol{A}$ = state coefficient matrix determining the unforced response of a system
$A(\Delta\theta)$ = coefficient describing response of MEMS actuator to an applied voltage
b = thickness of silicon leaf springs in MEMS actuator
$\boldsymbol{B}$ = state coefficient matrix determining the forced response of a system
C = generalized damping term for MEMS actuator
$\boldsymbol{d}$ = width of finger in comb drive for MEMS actuator
$\boldsymbol{d}_a$ = vector of artifact design variables
$\boldsymbol{d}_c$ = vector of control design variables
E_{PDMS} = Young's modulus for PDMS
E_{Si} = Young's modulus for silicon
f_a = artifact objective function
f_c = control objective function
$\boldsymbol{g}_a$ = artifact inequality constraints
$\boldsymbol{g}_c$ = control inequality constraints
$\boldsymbol{h}_1$ = thickness of micro-hinge
$\boldsymbol{h}_2$ = height of micro-hinge
$\boldsymbol{h}_a$ = artifact equality constraints
$\boldsymbol{h}_c$ = control equality constraints
k_b = beam end condition coefficient for micro-hinge in MEMS actuator
K = generalized spring constant for MEMS actuator
K_1, K_2, K_i = controller gains for MEMS actuator
l_1 = length of comb drive in MEMS actuator
l_{fo} = initial finger engagement in MEMS actuator
l_p = length of PDMS platform in MEMS actuator
l_{Si} = length of silicon springs in MEMS actuator
M = generalized inertia for MEMS actuator
n = number of fingers in comb drive in MEMS actuator
p = length of micro-hinge in MEMS actuator
t = width of micro-hinge in MEMS actuator
t_f = final time for interval of interest
u = control input applied to a system
V = voltage applied to comb drive in MEMS actuator
w = depth of micro-hinge in MEMS actuator
w_1 = weight attached to artifact objective function, f_a, in CPF problem formulation
w_2 = weight attached to Control Proxy Function, χ, in CPF problem formulation
w_a = Weight attached to artifact objective function, f_a, in simultaneous problem formulation
w_c = weight attached to control objective function, f_c, in simultaneous problem formulation
$\boldsymbol{W}_c(t_f)$ = Controllability Grammian matrix, evaluated at t_f
W_c^∞ = steady-state controllability Grammian matrix
$\boldsymbol{x}$ = state vector describing a system
$\boldsymbol{x_0}$ = state vector describing a system at $t = 0$
$\boldsymbol{x}_f$ = state vector describing a system at $t = t_f$
$\boldsymbol{\Gamma}_v$ = coupling vector
$\widehat{\boldsymbol{\Gamma}}_v$ = estimate of coupling vector
ε = distance between a given point in the $\boldsymbol{d}_a$-space and the nearest Pareto optimal point

ε_o = permittivity of vacuum
ζ = empirical parameter used in characterization of MEMS actuator
ΔX = horizontal displacement of comb drive in MEMS actuator
ΔZ = vertical displacement of MEMS actuator
$\Delta\theta$ = angular displacement of micro-hinge in MEMS actuator
$\boldsymbol{\lambda}$ = vector of Lagrange multipliers associated with equality constraints
$\boldsymbol{\mu}$ = vector of Lagrange multipliers associated with inequality constraints
ξ = angle between coupling vector and gradient of Control Proxy Function
$\sigma_{PDMS_{max}}$ = maximum allowable stress in PDMS
$\sigma_{Si_{max}}$ = maximum allowable stress in silicon
χ = Control Proxy Function (CPF)

References

[1] Haftka, R., Martinovic, Z., Jr., W. H., and Schamel, G., 1986, "An Analytical and Experimental Study of a Control System's Sensitivity to Structural Modifications," AIAA J., **25**, pp. 310–315.
[2] Rao, S., and Pan, T., 1990, "Modeling, Control, and Design of Flexible Structures: A Survey," Appl. Mech. Rev., **43**, pp. 99–117.
[3] Albers, A., and Ottnad, J., 2010, "Integrated Structural and Controller Optimization in Dynamic Mechatronic Systems," ASME J. Mech. Des., **132**, 041008.
[4] Carley, L., Ganger, G., Guillou, D., and Nagle, D., 2001, "System Design Considerations for MEMS-Actuated Magnetic-Probe-Based Mass Storage," IEEE Trans. Magn., **37**, pp. 657–662.
[5] Oldham, K., Huang, X., Chahwan, A., and Horowitz, R., 2005, "Design, Fabrication and Control of a High-Aspect Ratio Microactuator for Vibration Suppression in a Hard Disk Drive," *Proceedings of the IFAC World Congress*.
[6] Ravichandran, T., Wang, D., and Heppler, G., 2006, "Simultaneous Plant-Controller Design Optimization of a Two-Link Planar Manipulator," Mechatronics, **16**, pp. 233–242.
[7] Zhu, Y., Qiu, J., and Tani, J., 2001, "Simultaneous Optimization of a Two-Link Flexible Robot Arm," J. Rob. Syst., **18**(1), pp. 29–38.
[8] Udengaard, M., and Iagnemma, K., 2009, "Analysis, Design, and Control of an Omnidirectional Mobile Robot in Rough Terrain," ASME J. Mech. Des., **131**, 121002.
[9] Ou, J., and Kikuchi, N., 1996, "Integrated Optimal Structural and Vibration Control Design," Struct. Optim., **12**, pp. 209–216.
[10] Kosut, R., Kabuli, G., Morrison, S., and Harn, Y., 1990, "Simultaneous Control and Structure Design for Large Space Structures," *Proceedings of the American Control Conference, IEEE*, pp. 860–865
[11] Milman, M., Salama, M., Scheid, R., Bruno, R., and Gibson, J., 1991, "Combined Control-Structural Optimization," Comput. Mech., **8**, pp. 1–18.
[12] Sobieszczanski-Sobieski, J., and Haftka, R., 1997, "Multidisciplinary Aerospace Design Optimization: Survey of Recent Developments," Struct. Optim., **14**, pp. 1–23.
[13] Haftka, R., 1990, "Integrated Structure/Control Optimization of Space Structures," *Proceedings of the AIAA Dynamics Specialists Conference, AIAA*, pp. 1–9
[14] Fathy, H., Bortoff, S., Copeland, G., Papalambros, P. Y., and Ulsoy, A. G., 2002, "Nested Optimization of an Elevator and its Gain-Scheduled LQG Controller," *Proceedings of the ASME IMECE 2002, ASME*, pp. 119–126, Paper No. IMECE2002-34273.
[15] Bloebaum, C., 1995, "Coupling Strength-Based System Reduction for Complex Engineering Design," Struct.Optim., **10**, pp. 113–121.
[16] Fathy, H., Papalambros, P. Y., and Ulsoy, A. G., 2004, "On Combined Plant and Control Optimization," In 8th Cairo University International Conference on Mechanical Design and Production, Cairo University.
[17] Alyaqout, S. F., Papalambros, P. Y., and Ulsoy, A. G., 2005, "Quantification and use of System Coupling in Decomposed Design Optimization Problems," *Proceedings of the ASME IMECE 2005, ASME*, pp. 95–103, Paper No. IMECE2005-81364.
[18] Peters, D. L., Papalambros, P. Y., and Ulsoy, A. G., 2009, "On Measures of Coupling Between the Artifact and Controller Optimal Design Problems," *Proceedings of the ASME Design Engineering Technical Conference and Computers in Engineering Conference*, ASME, Paper No. DETC 2009-86868.
[19] Peters, D. L., 2010, "Coupling and Controllability in Optimal Design and Control," Ph.D. thesis, University of Michigan, Ann Arbor, MI.
[20] Fathy, H., Papalambros, P. Y., Reyer, J., and Ulsoy, A. G., 2001, "On the Plant and Controller Optimization Problems," Proceedings of the American Control Conference, ACC.
[21] Fathy, H., 2003, "Combined Plant and Control Optimization: Theory, Strategies and Applications," Ph.D. thesis, University of Michigan, Ann Arbor, MI.
[22] Reyer, J., 2000, "Combined Embodiment Design and Control Optimization: Effects of Cross-Disciplinary Coupling," PhD Thesis, University of Michigan, Ann Arbor, MI, April.
[23] Das, I., and Dennis, J., 1997, "A Closer Look at Drawbacks of Minimizing Weighted Sums of Objectives for Pareto Set Generation in Multicriteria Optimization Problems," Struct. Optim., **14**, pp. 63–69.
[24] Messac, A., and Puemi-Sukam, C., 2000, "Aggregate Objective Functions and Pareto Frontiers: Required Relationships and Practical Implications," Optim. Eng., **1**, pp. 171–188.
[25] Kitayama, S., Yamazaki, K., Arakawa, M., and Yamakawa, H., 2009, "Quantitative Trade-off Analysis and Its Application to the Compromise Solution in the Multi-Objective Design Optimization," *Proceedings of the 8th World Congress on Structural and Multidisciplinary Optimization*, WCSMO.
[26] Steuer, R. E., 1986, *Multiple Criteria Optimization: Theory, Computation and Application*, John Wiley and Sons, Inc., New York.
[27] Kuhn, H. W., and Tucker, A. W., 1950, "Nonlinear Programming," *Proceedings of the Second Berkeley Symposium on Mathematical Statistics and Probability*, University of California, pp. 481–492.
[28] Papalambros, P., and Wilde, D., 2000, *Principles of Optimal Design: Modeling and Computation*, Cambridge University Press, Cambridge, NY.
[29] Peters, D. L., Kurabayashi, K., Papalambros, P. Y., and Ulsoy, A. G., 2008, "Co-Design of a MEMS Actuator and Its Controller Using Frequency Constraints," Proceedings of the ASME Dynamic Systems and Control Conferences, ASME. Paper No. DSCC 2008-2212.
[30] Hale, A., Lisowski, R., and Dahl, W., 1985, "Optimal Simultaneous Structural and Control Design of Maneuvering Flexible Spacecraft," J. Guid., Control Dyn., **8**, pp. 86–93.
[31] Khot, N., and Abhyankar, N., 1993, "Integrated Optimum Structural and Control Design," In *Structural Optimization: Status and Promise*, M. P. Kamat, ed.
[32] Bodden, D., and Junkins, J., 1985, "Eigenvalue Optimization Algorithms for Structure/Controller Design Iterations," J. Guid., Control Dyn., **8**, pp. 697–706.
[33] Yee, E., and Tsuei, Y., 1991, "Method for Shifting Natural Frequencies of Damped Mechanical Systems," AIAA J., **29**(11), pp. 1973–1977.
[34] Peters, D. L., Papalambros, P. Y., and Ulsoy, A. G., 2010, "Sequential Co-Design of an Artifact and Its Controller via Control Proxy Functions," *Proceedings of the 5th IFAC Symposium on Mechatronic Systems*, IFAC.
[35] Peters, D. L., Papalambros, P. Y., and Ulsoy, A. G., 2010, "Relationship Between Coupling and the Controllability Grammian in Co-Design Problems," Proceedings of the American Control Conference, ASME.
[36] Skogestad, S., and Postlethwaite, I., 2005, *Multivariable Feedback Control: Analysis and Design*, John Wiley and Sons, Ltd., West Sussex, UK.
[37] Tung, Y., and Kurabayashi, K., 2005, "A Single-Layer PDMS-on-Silicon Hybrid Microactuator With Multi-Axis Out-of-Plane Motion Capabilities—Part I: Design and Analysis," J. Microelectromech. Syst., **14**(3), pp. 548–557.